ACS OMEGA

Open Access

http://pubs.acs.org/journal/acsodf

Article

High Volatile Antimony(III) Precursors for Metal Oxide Thin Film Deposition

Ji-Seoung Jeong, Sunyoung Shin, Bo Keun Park, Seung Uk Son, Taek-Mo Chung,* and Ji Yeon Ryu*

Cite This: *ACS Omega* 2024, 9, 31871−31877

Read Online

ACCESS | Metrics & More | Article Recommendations | Supporting Information

ABSTRACT: We report the synthesis and characterization of novel antimony(III) complexes: $Sb(mpa)_3$ (**1**), $Sb(mmpa)_3$ (**2**), $Sb(mdpa)_3$ (**3**), $Sb(epa)_3$ (**4**), $Sb(empa)_3$ (**5**), and $Sb(edpa)_3$ (**6**) (mpa = *N*-methoxypropanamide, mmpa = *N*-methoxy-2-methyl-propanamide, mdpa = *N*-methoxy-2,2-dimethylpropanamide, epa = *N*-ethoxypropanamide, empa = *N*-ethoxy-2-methylpropanamide, and edpa = *N*-ethoxy-2,2-dimethylpropanamide, via a salt-elimination reaction with $SbCl_3$ and sodium-substituted carboxamide. The molecular structure of **6** revealed the formation of a homoleptic conformer with a highly distorted pentagonal bipyramidal geometry, as determined by X-ray crystallography. Thermogravimetric analysis showed excellent volatility at elevated temperatures, with complex **4** displaying the lowest residual mass of 0.16% at 500 °C. For complexes **4**, **5**, and **6**, the temperature at a vapor pressure of 1 Torr and the enthalpy of vaporization were estimated to be 58, 64, and 45 °C and 83.31, 103.58, and 99.93 kJ/mol, respectively.

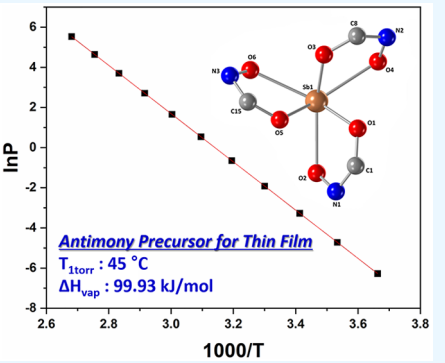

INTRODUCTION

Thin films containing antimony (such as oxides, nitrides, sulfides, and chalcogenides) have gained considerable interest owing to their various applications, such as catalysts for photoelectrochemical water-splitting,[1] anode materials for lithium-ion batteries,[2] light sensitizers for solar cells,[3] and ultraviolet filters for interferometric applications.[4,5] Among antimony oxides, antimony trioxide (Sb_2O_3) has excellent electrical properties, good transparency, a high refractive index (2.0−2.5), a wide band gap (>3.4 eV), and a high breakdown voltage (~5.7 GV m^{-1}), making it suitable for a wide range of applications, including gas sensors,[6,7] dielectric mirror systems for the UV region,[4] electronic devices, and thin film transistors (TFTs).[8,9]

Antimony trioxide thin films have been previously prepared by thermal sputtering,[10] thermal evaporation,[11] chemical vapor deposition (CVD),[6,12] and atomic layer deposition (ALD).[13,14] The fabrication method significantly influences the morphological and chemical properties of the thin films. In particular, ALD is a powerful thin-film deposition technique owing to its precise control of film thickness and excellent reproducibility as well as high-quality conformality on a variety of substrates, all of which are essential for most of the aforementioned applications.[15]

Volatility and thermal stability are prerequisites for CVD and ALD precursors for transportation and deposition. Therefore, the design and synthesis of precursors are important to ensure properties, such as a low melting point, high vapor pressure, high volatility, good thermal stability, and self-limiting reactivity. The antimony(III) precursor for the CVD process was first synthesized by Horley et al. in 2002 using tris(dimethylamino)antimony(III) and 2,6-dimethylphenol in dry hexane via the Schlenk technique.[16] Horley et al. prepared homoleptic antimony carbamate complexes ($Sb(O_2CNR)_3$, where R = Me, Et, Pr^i) and used $Sb(O_2CNMe_2)_3$ as a single-source precursor in the low-pressure chemical vapor deposition of Sb_2O_3 thin films. Although these precursors have sensitivity to moist air and sufficient volatility, they require deposition at a high temperature of approximately 400 °C.[17] Yang et al. described ALD processes using a trivalent antimony precursor $Sb(NMe_2)_3$ and ozone, resulting in Sb_2O_5 thin films.[13] Recently, Yang et al. reported that $Sb(NMe_2)_3$ and H_2O_2 via low-temperature ALD processes generated a mixture of Sb_2O_5 and Sb_2O_3, in which high deposition temperature increased the Sb_2O_3 phase in the thin film.[9]

This study focuses on synthesizing novel antimony precursors with improved properties for thin film deposition. Metal precursors utilizing alkoxy-modified carboxamide ligands have been widely investigated in our group for thin film deposition.[18−20] Three monoanionic bidentate carboxamide ligands were employed to satisfy the oxidation number and binding site of antimony(III). Additionally, tuning the pendant group at the α carbon position and the oxygen atom of the amide group effectively reduced interactions between mole-

Received: April 11, 2024
Revised: July 2, 2024
Accepted: July 5, 2024
Published: July 15, 2024

cules, resulting in a high vapor pressure and a low melting point.

To develop novel antimony precursors, we synthesized six Sb(III) carboxamide complexes, $Sb(mpa)_3$ (**1**), $Sb(mmpa)_3$ (**2**), $Sb(mdpa)_3$ (**3**), $Sb(epa)_3$ (**4**), $Sb(empa)_3$ (**5**), and $Sb(edpa)_3$ (**6**), as potential precursors for Sb-based thin films. All complexes were characterized by Fourier transform infrared (FT-IR) spectroscopy, nuclear magnetic resonance (NMR), elemental analysis (EA), and thermogravimetric analysis (TGA). Complex **6** was subjected to a single crystal X-ray diffraction (SCXRD), as well as density functional theory (DFT) calculations. For **5** and **6**, vapor pressure was performed using a dynamic method.

RESULTS AND DISCUSSION

Synthesis and Characterization. Antimony complexes **1**−**6** were synthesized via a salt-elimination reaction with 1 equiv of $SbCl_3$ and 3.2 equiv of sodium-substituted ***L*1**Na−***L*6**Na in toluene (Scheme 1). For all reactions, the mixture

Scheme 1. Synthetic Route of Sb Complexes 1−6

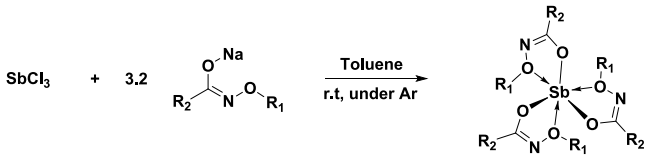

1: R_1=Me, R_2=Et
2: R_1=Me, R_2=^{i}Pr
3: R_1=Me, R_2=^{t}Bu
4: R_1=Et, R_2=Et
5: R_1=Et, R_2=^{i}Pr
6: R_1=Et, R_2=^{t}Bu

gradually became cloudy with the addition of the ligand solution into the metal solution, indicating the progress of the reaction. All complexes were stable under inert conditions, such as a nitrogen or argon atmosphere. The prepared complexes had a high solubility in chlorinated organic solvents as well as benzene, hexane, THF, and diethyl ether. The crude product $Sb(\boldsymbol{L1})_3$-$Sb(\boldsymbol{L6})_3$ was easily isolated as a colorless liquid of **1**, **2**, and **4**, a white solid of **3** and **6**, and a yellow solid of **5** after filtration, followed by the removal of volatile chemicals. The purification of the final products was accomplished by distillation (**1**, **2**, **4**, and **5**), sublimation (**3**), or recrystallization (**6**) from the hexane solution. Final complexes were characterized by various methods, including NMR spectroscopy, EA, IR spectroscopy, and X-ray crystallography.

The ^{1}H NMR spectrum of **1**−**6** in $CDCl_3$ solution showed diagnostic shifts without concomitant formation of side products (Figures S7−S18 in the Supporting Information). For **1**−**3**, the methoxy group shifted upfield compared with that of the free ligands (from 3.83 to 3.66 ppm of **1**, from 3.62 to 3.78 ppm of **2**), whereas **3** was shifted downfield from 3.66 to 3.77 ppm. The OCH_2CH_3 of the ethoxy group in **4**−**6** shifted downfield relative to those of the relevant starting materials ***L*4**−***L*6** (from 3.93 to 4.08 ppm for **4**, from 3.86 to 4.06 ppm for **5**, and from 3.86 to 4.06 ppm for **6**), thereby indicating that the oxygen in the electron donor was coordinated to the antimony atom. The imine peak of all complexes in the ^{13}C NMR spectrum showed peaks in the range of 163.66−168.38; this range is similar to that observed for previously reported homoleptic metal monomer complexes using these types of ligands.[18,19] These observations confirmed that the ligand was attached via a desalted oxygen atom to the antimony metal center.

Crystal Structure. To further establish the chemical identity of **6**, single crystals suitable for X-ray diffraction were grown from a saturated hexane solution at 30 °C. The selected bond distances and angles are listed in Table 1. The

Table 1. Selected Bond Lengths (Å) and Bond Angles (deg) for Complex 6

bond lengths (Å)		bond angles (deg)	
Sb1−O1	2.0248(14)	O5−Sb1−O3	85.41(6)
Sb1−O2	2.5274(14)	O1−Sb1−O3	88.37(6)
Sb1−O3	2.0251(15)	O5−Sb1−O2	76.99(5)
Sb1−O4	2.5822(14)	O3−Sb1−O6	78.65(5)
Sb1−O5	2.0232(14)	O2−Sb1−O6	114.52(5)
Sb1−O6	2.5441(14)	O2−Sb1−O4	120.11(5)
bite angles		trans angles	
O1−Sb1−O2	66.55(5)	O1−Sb1−O6	149.14(5)
O3−Sb1−O4	65.61(5)	O2−Sb1−O3	150.18(5)
O5−Sb1−O6	66.07(5)	O5−Sb1−O4	146.15(5)
others		ligand dihedral angels	
O5−Sb1−O1	85.23(6)	O2−N1−C1−O1	1.4(3)
O1−Sb1−O4	77.20(5)	O4−N2−C8−O3	2.0(3)
O6−Sb1−O4	120.68(5)	O6−N3−C15−O5	1.1(3)

mononuclear antimony complex **6** crystallizes in a monoclinic $P2_1/n$ space group with four molecules in a unit cell. The obtained antimony(III) complex showed a homoleptic monomeric conformer in a solid-state structure. The mononuclear Sb atom was surrounded via seven coordinates with three ligand molecules chelated via a κ^2-O2 binding mode and a lone pair of electrons. The coordination polyhedron defined by the atoms directly bonding to antimony can be described as a highly distorted pentagonal bipyramidal geometry, in which O2 and O3 occupy axial positions (O3−Sb−O2; 150.18(5)°), and O1, O4, O5, and O6 and a lone pair of electrons occupy the equatorial plane.[21] The angles of O−Sb−O located in the equatorial plane vary from 66.07(5)° to 85.23(6)°, and those of E−Sb−O (where E represents the electron pair) centered on the lone pair between O4 and O6 were estimated to be 59.59(6)° and 61.09(6)°, respectively. The bite angles of O−Sb−O also exhibited a narrow range from 65.61(5)° to 66.55(5)°; those of O−Sb−O (trans) ranged from 146.15(5)° to 150.18(5)°. Ligand dihedral angles (OCNO) within the five-membered chelate ring were 1.4(3)° for O(1)−O(2), 2.0(3)° for O(3)−O(4), and 1.1(3)° for O(5)−O(6). The sum of the angles at ONCO planes from chelated ligands in **6** was 329.09°; it tilted by an average of 86.9° in the same direction, leading to a propeller-like conformation for minimizing steric interactions. As shown in Figure 1, the bond distances between the Sb metal center and oxygen atoms contributed by the ligand molecule vary from 2.023 to 2.582 Å due to the unsymmetrical chelation mode, as is evident from the two sets of Sb−O_{long} and Sb−O_{short} bonds. The Sb−O covalent bond distances, ranging from 2.023(14) to 2.025(15) Å, are shorter than those of the coordinate bonds, ranging from 2.527(14) to 2.582(14), with the longest bond being adjacent to the lone pair at the equatorial position. Also, the Sb−O bond distances in **6** are similar to those reported antimony(III) β-diketonate complexes composed of three five-

https://doi.org/10.1021/acsomega.4c03482
ACS Omega 2024, 9, 31871−31877

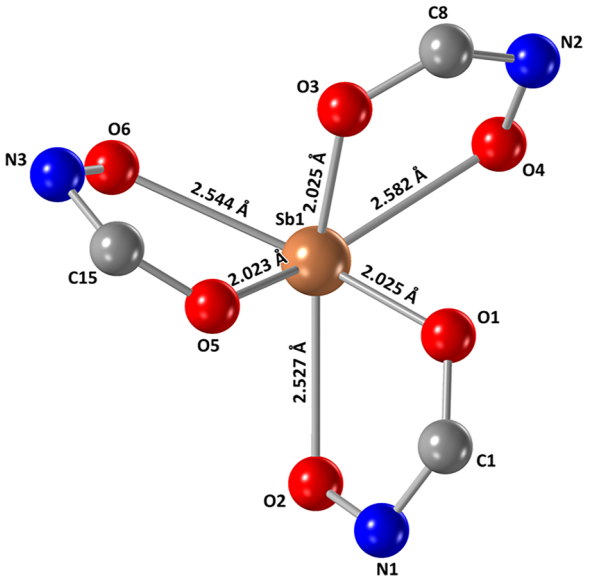

Figure 1. Highlighted bond lengths of complex **6** from X-ray crystal structures with thermal ellipsoids at the 50% probability level. Alkyl chains and hydrogen atoms are not shown for visual clarity (gold, antimony; blue, nitrogen; red, oxygen; gray, carbon).

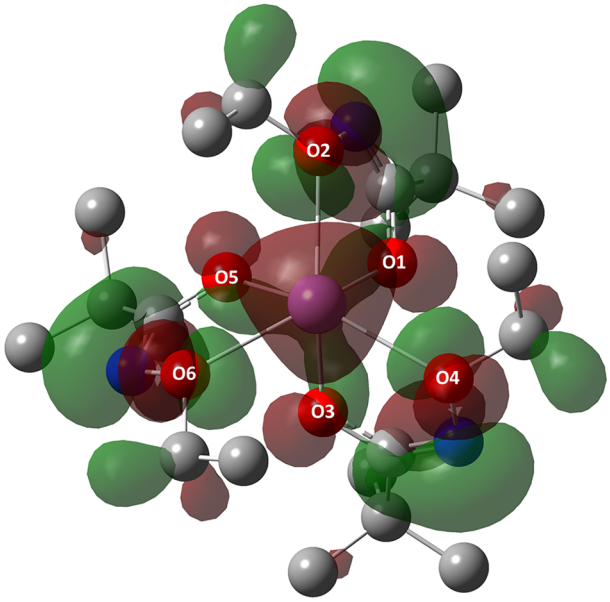

Figure 2. Top view of the HOMO energy level of the optimized molecular structure of complex **6** from DFT calculations. Hydrogen atoms are not shown for visual clarity (purple, antimony; blue, nitrogen; red, oxygen; gray, carbon).

membered metallacycles based on 2,2,6,6-tetramethyl-3,5-heptanedione (thd) with a κ^2-O2 binding mode.[22] The Sb–O lengths in $Sb(thd)_3$ range from 2.446(3) to 2.468(3) for $Sb-O_{long}$ and from 2.055(3) to 2.065(3) for $Sb-O_{short}$.

Theoretical Calculations. Theoretical calculations were performed using the *Gaussian 16* software to investigate the stability of the structure and the presence of a lone pair of electrons between O4 and O6. The geometry of the ground state of **6** was optimized in a chloroform solution at the B3LYP functional[23] and 6-31G** basis set[24] for nonmetal atoms and SBKJC VDZ ECP basis set[25] for Sb atoms. As shown in Figure 2, a lone pair of electrons exists between the orbitals of O4 and O6 at the equatorial plane. Distortion from ideal geometry on metal center showed somewhat narrow O–Sb–O trans angles attributable to the lone electron pair. The bond angles of O–Sb–O (trans) were calculated as 146.40° (O1–Sb1–O6, equatorial), 146.45° (O2–Sb1–O3, axial), and 146.39° (O4–Sb1–O5, equatorial), respectively. Based on these results, the DFT calculations predicted that complex **6** possesses a highly distorted pentagonal bipyramidal geometry, which agrees with the molecular structure observed from single-crystal X-ray diffraction shown in Figure 1. Selected bond lengths (Å) and angles (deg) for **6** are listed in Table S3.

Thermal Analysis. The thermal behavior and volatility of **1**–**6** were explored using TGA in the temperature range of 30–500 °C under a constant flow of nitrogen. The physical properties and TGA traces of **1**–**6** are shown in Table 2 and Figure 3, respectively. The TGA trace of **2** and **5** show three-step weight losses, with the first weight loss of approximately 20% at 157 °C for **2** and 170 °C for **5**. The greatest weight loss occurred between 150 and 190 °C, and the third step occurred between 430 and 500 °C with nonvolatile residues of 7.0% for **2** and 17.2% for **5**. The TGA traces of **3** and **6** showed two-step weight losses; the onset of mass loss occurred at 89 °C for **3** and 106 °C for **6**. Complexes **3** and **6** showed considerable weight loss up to their decomposition temperatures (203–216 °C) and small weight loss at 400–500 °C, with nonvolatile residues of 11.9% for **3** and 5.9% for **6**. **1** and **4** show single-step weight losses starting at approximately 120 °C. A weight loss of approximately 50% was observed at 201 °C for **1** and 209 °C for **4**. The percent nonvolatile residue for **4** up to 500 °C was the lowest among the six complexes (nonvolatile residues of **4** < **1**, **2**, **6** < **3** < **5**).

Table 2. Physical Properties of Complexes 1–6

complex	formula	mol wt (g/mol)	melting point (°C)	onset of mass loss[a] (°C)	residual mass[b] (%)
1	$C_{12}H_{24}N_3O_6Sb$	428.10		117	6.4
2	$C_{15}H_{30}N_3O_6Sb$	470.18	48.6	100	7.0
3	$C_{18}H_{36}N_3O_6Sb$	512.26	55.3	89	11.9
4	$C_{15}H_{30}N_3O_6Sb$	470.18		123	0.16
5	$C_{18}H_{36}N_3O_6Sb$	512.26	34.6	114	17.2
6	$C_{21}H_{42}N_3O_6Sb$	554.34	80.7	106	5.9

[a]Temperature at 2% mass loss. [b]Residual mass at 500 °C.

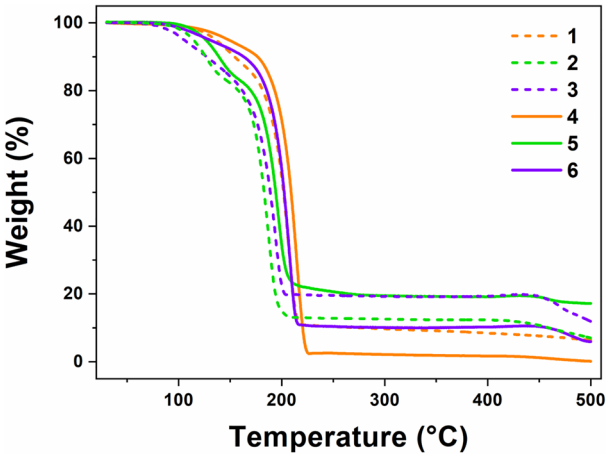

Figure 3. Thermogravimetric analysis (TGA) traces of complexes **1**–**6** at a heating rate of 10 °C/min.

https://doi.org/10.1021/acsomega.4c03482
ACS Omega 2024, 9, 31871–31877

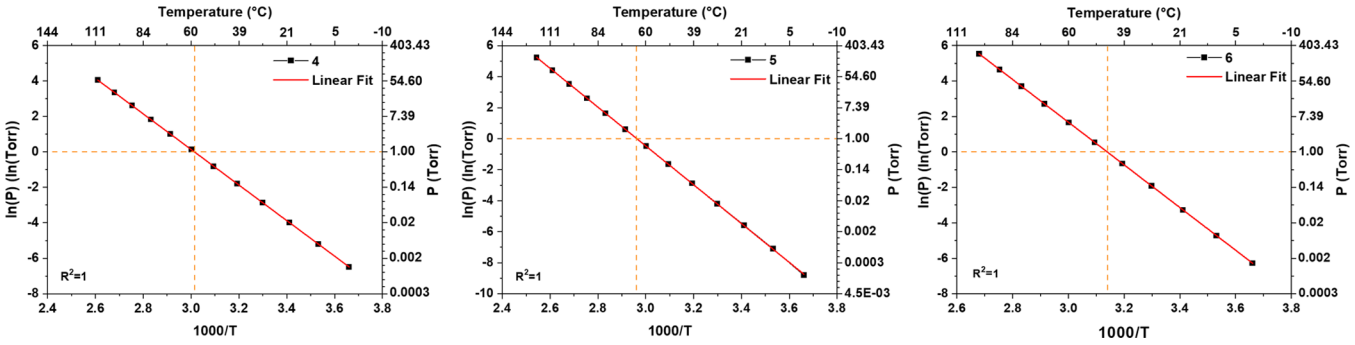

Figure 4. Vapor pressure ($\ln P$) versus temperature ($1000/T$) plots for complexes **4**, **5**, and **6**.

Vapor Pressure Measurement. Vapor pressure was measured to determine the volatilities of **4**, **5**, and **6** (Figure 4). The vapor pressure−temperature correlation can be described by eqs 1, 2, and 3 for complexes **4**, **5**, and **6**, respectively.

$$\ln P = -10021/T + 30.219 \quad (1)$$

$$\ln P = -12459/T + 36.927 \quad (2)$$

$$\ln P = -12020/T + 37.752 \quad (3)$$

Here, P is the pressure in Torr and T is the temperature in K. The vapor pressures at 30 °C for **4**, **5**, and **6** were measured to be 0.05, 0.015, and 0.14 Torr, respectively; thus, **6** is 10 times more volatile than **5**. The temperature values at 1 Torr vapor pressure, which are often used as a comparison target for the precursor volatility in industrial applications, were 58 °C for **4**, 64 °C for **5**, and 45 °C for **6**; these temperature values are lower than those for commonly known precursors, except for tris(dimethylamido)antimony(III). The vapor pressure of commercial precursors are as follows. $SbCl_3$: 1 Torr at 50 °C;[26] $Sb(OCH_2CH_3)_3$: 1 Torr at 95 °C;[27] $[(CH_3)_3Si]_3Sb$: 0.15 Torr at 40 °C;[28] $Sb[N(CH_3)_2]_3$: 1.04 Torr at 30 °C.[29] The enthalpy of vaporization from the Clausius−Clapeyron equation was estimated to be 83.31, 103.58, and 99.93 kJ/mol for **4**, **5**, and **6**, respectively.

CONCLUSION

Six homoleptic Sb(III) complexes, $Sb(mpa)_3$ (**1**), $Sb(mmpa)_3$ (**2**), $Sb(mdpa)_3$ (**3**), $Sb(epa)_3$ (**4**), $Sb(empa)_3$ (**5**), and $Sb(edpa)_3$ (**6**), were successfully synthesized and characterized. Complexes **1**, **2**, **4**, and **5** were distilled at 50 °C under 0.7 Torr, at 120 °C under 0.9 Torr, at 70 °C under 0.6 Torr, and at 75 °C under 0.6 Torr, respectively. Complexes **3** and **6** were sublimed at 70 and 80 °C under 0.4 and 0.6 Torr, respectively. X-ray crystallography and theoretical calculations confirmed that the molecular structure of **6** showed seven-coordination with three ligand molecules chelated via a κ^2-O2 binding mode and a lone pair of electrons. The geometry was described as a highly distorted pentagonal bipyramidal geometry. In TGA traces, complexes **2**, **3**, **5**, and **6** showed multistep weight loss, whereas **1** and **4** showed single-step weight loss. The nonvolatile residues of **1**−**6** at 500 °C ranged from 0.16% to 17.2%. The temperature at a vapor pressure of 1 Torr and the enthalpy of vaporization for **4**, **5**, and **6** were calculated to be 58 °C and 83.31 kJ/mol, 64 °C and 103.58 kJ/mol, and 45 °C and 99.93 kJ/mol, respectively. Based on these physicochemical properties, these complexes are promising materials for thin film growth via ALD. Further studies of antimony oxide thin films using complex **6**, which had the lowest temperature values at 1 Torr vapor pressure, are in progress.

EXPERIMENTAL SECTION

General Synthetic Procedures. All commercially available chemicals were used as received. Air-sensitive reactions were performed in an inert atmosphere of argon using standard Schlenk and glovebox techniques. All anhydrous-grade solvents (*n*-hexane and toluene) were purified by a Pure Solv-MD solvent purification system from the Innovative Technology, Inc. ^1H and ^{13}C spectra were recorded on a Bruker DPX 400 MHz FT-NMR spectrometer (400 MHz for ^1H, 101 MHz for ^{13}C) at ambient temperature. Infrared (IR) spectra were measured in the range of 4000−400 cm^{-1} with KBr pellets on Bruker ALPHA II spectrometer. Melting points were measured using open-ended capillaries on an electrothermal melting point apparatus and are uncorrected. All TGA experiments were conducted on a TGA 2 instrument in Mettler Toledo inside of 10 °C/min to a maximum temperature of 500 °C with mass loadings of ∼10 mg. All measurements were conducted nonisothermally. Elemental analyses were performed by using a Thermo Scientific Flash 2000 CHNS analyzer. The ligands ***L*1**Na−***L*6**Na were modified using previously reported procedures.[18,30]

*Synthesis of $Sb(mpa)_3$ (**1**).* Na(mpa) (1.00 g, 8.00 mmol, 3.2 equiv) was added dropwise to a solution of $SbCl_3$ (0.570 g, 2.50 mmol, 1.0 equiv) in toluene (20 mL) at room temperature, and the reaction mixture was stirred for 24 h under an argon atmosphere. The mixture was filtered through fritted glass filter, the volatile solvent in the filtrate was removed under reduce pressure to produce the desired product as a colorless liquid. The crude product was purified by distillation to obtain residue product of colorless liquid. Yield: 47.9%. Distillation: 50 °C/0.7 Torr. ^1H NMR (400 MHz, $CDCl_3$) δ (ppm): 3.75−3.54 (m, J = 20.5 Hz, 9H, OCH_3), 2.24−1.92 (m, 6H, CH_2CH_3), 1.08−0.91 (m, 9H, CH_2CH_3). ^{13}C NMR (101 MHz, $CDCl_3$) δ (ppm): 163.70, 60.04, 24.79, 10.60. Anal. calcd for $C_{12}H_{24}N_3O_6Sb$: C, 33.67; H, 5.65; N, 9.82. Found: C, 33.82; H, 5.66; N, 9.28. FT-IR (KBr, cm^{-1}): 2978 (s), 2941 (s), 2904 (m), 2881 (m), 2818 (w), 1657 (w), 1614 (s), 1464 (s), 1437 (m), 1377 (m), 1346 (s), 1281 (s), 1257 (s), 1189 (m), 1060 (s), 1037 (s), 999 (s), 933 (m), 854 (m), 797 (w), 710 (w), 629 (m), 496 (w), 451 (m).

*Synthesis of $Sb(mmpa)_3$ (**2**).* Na(mmpa) (0.700 g, 5.03 mmol, 3.2 equiv) was added dropwise to a solution of $SbCl_3$ (0.359 g, 1.57 mmol, 1.0 equiv) in toluene (30 mL) at room temperature, and the reaction mixture refluxed for 24 h under argon atmosphere. The mixture was filtered through fritted

https://doi.org/10.1021/acsomega.4c03482
ACS Omega 2024, 9, 31871−31877

glass filter, the volatile solvent in the filtrate was removed under reduce pressure to produce the desired product as a gray liquid. The crude product was purified by distillation to obtain product of colorless liquid. Yield: 74.4%. m.p: 48.6 °C. Distillation: 120 °C/0.9 Torr. ^{1}H NMR (400 MHz, $CDCl_3$) δ (ppm): 3.78 (s, 9H, OCH_3), 2.53 (p, J = 6.9 Hz, 3H, $CCH(CH_3)_2$), 1.11 (d, J = 6.9 Hz, 18H, $CCH(CH_3)_2$). ^{13}C NMR (101 MHz, $CDCl_3$) δ(ppm): 166.73, 60.11, 31.25, 19.89. Anal. Calcd For $C_{15}H_{30}N_3O_6Sb$: C, 38.32; H, 6.43; N, 8.94. Found: C, 38.17; H, 6.49; N, 8.61. FT-IR (KBr, cm^{-1}): 2974 (s), 2940 (s), 2903 (s), 2875 (s), 2822 (m), 1645 (s), 1604 (s), 1469 (s), 1440 (m), 1386 (s), 1336 (s), 1282 (s), 1256 (s), 1190 (s), 1163 (m), 1075 (s), 1040 (s), 950 (s), 892 (s), 840 (m), 822 (s), 723 (m), 678 (s), 614 (s), 582 (m), 482 (s), 458 (m).

*Synthesis of Sb(mdpa)$_3$ (**3**).* In a manner analogous to the procedure for **1**, Na(mdpa) (0.49 g, 3.20 mmol, 3.2 equiv) was added dropwise to a solution of $SbCl_3$ (0.228 g, 1.00 mmol, 1.0 equiv) in toluene (20 mL). The crude product was purified by sublimation to give a white solid. Yield: 93.8%. m.p: 55.3 °C. Sublimation: 70 °C/0.4 Torr. ^{1}H NMR (400 MHz, $CDCl_3$) δ (ppm): 3.77 (s, 9H, OCH_3), 1.16 (s, 27H, $C(CH_3)_3$). ^{13}C NMR (101 MHz, $CDCl_3$) δ (ppm): 168.38, 60.05, 36.32, 27.80. Anal. calcd for $C_{18}H_{36}N_3O_6Sb$: C, 42.20; H, 7.08; N, 8.20. Found: C, 42.37; H, 7.45; N, 8.00. FT-IR (KBr, cm^{-1}): 2974 (s), 2962 (s), 2937 (s), 2905 (s), 2869 (s), 2816 (m), 1653 (s), 1599 (s), 1482 (s), 1461 (s), 1394 (s), 1365 (s), 1323 (s), 1227 (s), 1182 (s), 1047 (s), 937 (m), 917 (m), 864 (s), 810 (w), 796 (m), 726 (m), 618 (s), 543 (m), 481 (s), 429 (w).

*Synthesis of Sb(epa)$_3$ (**4**).* In a manner analogous to the procedure for **1**, Na(epa) (1.00 g, 7.19 mmol, 3.2 equiv) was added dropwise to a solution of $SbCl_3$ (0.512 g, 2.25 mmol, 1 equiv) in toluene (20 mL). The crude product was purified by distillation to obtain product of colorless liquid. Yield: 77.9%. Distillation: 70 °C/0.6 Torr. ^{1}H NMR (400 MHz, $CDCl_3$) δ (ppm): 4.08 (q, J = 7.1 Hz, 6H,OCH_2CH_3), 2.20 (q, J = 7.5 Hz, 6H, CH_2CH_3), 1.30 (t, J = 7.1 Hz, 9H, OCH_2CH_3), 1.11 (t, J = 7.5 Hz, 9H, CH_2CH_3). ^{13}C NMR (101 MHz, $CDCl_3$) δ (ppm): 163.66, 69.31, 25.30, 15.04, 10.96. Anal. calcd for $C_{15}H_{30}N_3O_6Sb$: C, 38.32; H, 6.43; N, 8.94. Found: C, 38.65; H, 6.49; N, 8.76. FT-IR (KBr, cm^{-1}): 2976 (s), 2939 (s), 2892(s), 2726 (w), 1665 (m), 1610 (s), 1462 (s), 1380 (s), 1346 (s), 1280 (s), 1252 (s), 1169 (m), 1125 (s), 1046 (s), 1002 (s), 944 (m), 922 (s), 900 (s), 850 (m), 800 (m), 708 (m), 631 (s), 495 (m), 459 (w), 429 (m).

*Synthesis of Sb(empa)$_3$ (**5**).* In a manner analogous to the procedure for **2**, Na(empa) (1.50 g, 9.79 mmol, 3.2 equiv) was added dropwise to a solution of $SbCl_3$ (0.698 g, 3.06 mmol, 1.0 equiv) in toluene (30 mL). The crude product was purified by distillation to obtain the residue product of a yellow solid. Yield: 94.7%. m.p: 34.6 °C. Distillation: 75 °C/0.6 Torr. ^{1}H NMR (400 MHz, $CDCl_3$) δ (ppm): 4.06 (q, J = 7.1 Hz, 6H, OCH_2CH_3), 2.51 (p, J = 6.8 Hz, 3H, $CCH(CH_3)_2$), 1.29 (t, J = 7.1 Hz, 9H, OCH_2CH_3), 1.09 (d, J = 6.8 Hz, 18H, $CCH(CH_3)_2$). ^{13}C NMR (101 MHz, $CDCl_3$) δ (ppm): 166.19, 69.22, 31.36, 19.89, 15.06. Anal. calcd for $C_{18}H_{36}N_3O_6Sb$: C, 42.20%; H, 7.08%; N, 8.20%. Found: C, 41.60%; H, 7.08%; N, 7.94%. FT-IR (KBr, cm^{-1}): 2973 (s) 2935 (s), 2893 (m), 2876 (m), 2810 (w), 1656 (m), 1609 (s), 1471 (m), 1385 (s), 1335 (s), 1280 (s), 1256 (m), 1165 (m), 1125 (s), 1094 (s), 1075 (s), 1047 (s), 969 (m), 919 (s), 897 (m), 823 (m), 791 (w), 722 (m), 675 (m), 617 (m), 514 (w), 475 (m), 433 (w).

*Synthesis of Sb(edpa)$_3$ (**6**).* In a manner analogous to the procedure for **1**, Na(edpa) (1.03 g, 6.17 mmol, 3.1 equiv) was added dropwise to a solution of $SbCl_3$ (0.440 g, 1.93 mmol, 1 equiv) in toluene (40 mL). X-ray quality crystals were grown from hexane by slow evaporation at room temperature. Yield: 76.4%. m.p: 80.7 °C. Sublimation: 80 °C/0.6 Torr. ^{1}H NMR (400 MHz, $CDCl_3$) δ (ppm): 4.06 (q, J = 7.0 Hz, 6H, OCH_2CH_3), 1.29 (t, J = 7.0 Hz, 9H, OCH_2CH_3), 1.15 (s, 27H, $C(CH_3)_3$). ^{13}C NMR (101 MHz, $CDCl_3$) δ (ppm): 167.72, 69.21, 36.40, 27.82, 15.12. Anal. calcd for $C_{21}H_{42}N_3O_6Sb$: C, 45.50; H, 7.64; N, 7.58. Found: C, 45.40; H, 7.97; N, 7.42. FT-IR (KBr, cm^{-1}): 2977 (s), 2936 (s), 2893 (s), 2872 (m), 2808 (w), 1650 (m), 1601 (s), 1483 (s), 1458 (m), 1386 (s), 1360 (m), 1323 (s), 1261 (w), 1225 (m), 1183 (s), 1160 (m), 1123 (s), 1093 (m), 1046 (s), 962 (m), 941 (m), 922 (s), 864 (m), 812, (w), 795 (w), 724 (w), 633 (m), 616 (s), 574 (w), 510 (w), 472 (m), 440 (w), 416 (w).

Crystallography. Single crystals of complex **6** were prepared from saturated hexane solutions at room temperature. Reflection data for **6** were collected by using a Bruker SMART Apex II-CCD area detector diffractometer with graphite-monochromated MoKα radiation (λ = 0.71073 Å). The hemisphere of the reflection data was collected as ω scan frames at 0.3° per frame and an exposure time of 10 s per frame. The cell parameters were determined and refined by using the APEX2 program.[31] The data were corrected for Lorentz and polarization effects. An empirical absorption correction was applied using the SADABS program.[32] The structures of the complexes were solved using direct methods and refined by full-matrix least-squares methods using the SHELXTL program package[33] and Olex2[34] with anisotropic thermal parameters for all nonhydrogen atoms. The data are summarized in Table S1. CCDC 2323975 for complex **6** contains the supplementary crystallographic data for this study. These data can be obtained free of charge from The Cambridge Crystallographic Data Centre via www.ccdc.cam.ac.uk/data_request/cif

Theoretical Calculation. Theoretical calculations of complex **6** were performed using *Gaussian 16* software[35] on a supercomputer (KISTI, Neuron). The initial structure of **6** was based on the obtained X-ray crystal structure and the molecular structures was optimized in chloroform solution at the B3LYP/SBKJC VDZ ECP level of theory.

Vapor Pressure of 4, 5, and 6. The vapor pressures of complexes **4**, **5**, and **6** were measured in accordance with OECD Test Guideline 104 at the Korea Polymer Testing and Research Institute (Koptri).

■ ASSOCIATED CONTENT

Supporting Information

The Supporting Information is available free of charge at https://pubs.acs.org/doi/10.1021/acsomega.4c03482.

Spectral data (IR, ^{1}H, ^{13}C NMR) of **1**−**6**, X-ray data collection and structure refinement for **6**, and selected bond lengths and bond angles of **6** with DFT data, and ln P vs 1/T graph of **5** and **6** (PDF)

Crystallographic data for **6** (CIF)

Accession Codes

CCDC 2323975 contain the supplementary crystallographic data for this paper. These data can be obtained free of charge

https://doi.org/10.1021/acsomega.4c03482
ACS Omega 2024, 9, 31871−31877

via www.ccdc.cam.ac.uk/data_request/cif, or by emailing data_request@ccdc.cam.ac.uk, or by contacting The Cambridge Crystallographic Data Centre, 12 Union Road, Cambridge CB2 1EZ, UK; fax: + 44 1223 336033.

AUTHOR INFORMATION

Corresponding Authors

Taek-Mo Chung − *Thin Film Materials Research Center, Korea Research Institute of Chemical Technology, Daejeon 34114, Republic of Korea; Advanced Materials and Chemical Engineering, KRICT School, University of Science and Technology (UST), Daejeon 34114, Republic of Korea;* orcid.org/0000-0002-5169-2671; Email: tmchung@krict.re.kr

Ji Yeon Ryu − *Thin Film Materials Research Center, Korea Research Institute of Chemical Technology, Daejeon 34114, Republic of Korea;* orcid.org/0000-0001-6321-5576; Email: jy.ryu@krict.re.kr

Authors

Ji-Seoung Jeong − *Thin Film Materials Research Center, Korea Research Institute of Chemical Technology, Daejeon 34114, Republic of Korea; Department of Chemistry, Sungkyunkwan University (SKKU), Gyeonggi-do 16419, Republic of Korea*

Sunyoung Shin − *Thin Film Materials Research Center, Korea Research Institute of Chemical Technology, Daejeon 34114, Republic of Korea*

Bo Keun Park − *Thin Film Materials Research Center, Korea Research Institute of Chemical Technology, Daejeon 34114, Republic of Korea; Advanced Materials and Chemical Engineering, KRICT School, University of Science and Technology (UST), Daejeon 34114, Republic of Korea;* orcid.org/0000-0002-4066-0500

Seung Uk Son − *Department of Chemistry, Sungkyunkwan University (SKKU), Gyeonggi-do 16419, Republic of Korea;* orcid.org/0000-0002-4779-9302

Complete contact information is available at: https://pubs.acs.org/10.1021/acsomega.4c03482

Notes

The authors declare no competing financial interest.

ACKNOWLEDGMENTS

We gratefully acknowledge the financial support from the Development of Smart Chemical Materials for IoT Devices Project (KS2321-10) through the Korea Research Institute of Chemical Technology and the National R&D Program through the National Research Foundation of Korea (NRF) funded by Ministry of Science and ICT (2020M3H4A3081866).

REFERENCES

(1) DeAngelis, A. D.; Kemp, K. C.; Gaillard, N.; Kim, K. S. Antimony(III) Sulfide Thin Films as a Photoanode Material in Photocatalytic Water Splitting. *ACS Appl. Mater. Interfaces* **2016**, *8* (13), 8445−8451.

(2) Sun, Q.; Li, W.-J.; Fu, Z.-W. A novel anode material of antimony nitride for rechargeable lithium batteries. *Solid State Sci.* **2010**, *12* (3), 397−403.

(3) Choi, Y. C.; Mandal, T. N.; Yang, W. S.; Lee, Y. H.; Im, S. H.; Noh, J. H.; Seok, S. I. Sb_2Se_3-Sensitized Inorganic-Organic Heterojunction Solar Cells Fabricated Using a Single-Source Precursor. *Angew. Chem., Int. Ed.* **2014**, *53* (5), 1329−1333. Liu, X.; Chen, J.; Luo, M.; Leng, M.; Xia, Z.; Zhou, Y.; Qin, S.; Xue, D.-J.; Lv, L.; Huang, H.; et al. Thermal Evaporation and Characterization of Sb_2Se_3 Thin Film for Substrate Sb_2Se_3/CdS Solar Cells. *ACS Appl. Mater. Interfaces* **2014**, *6* (13), 10687−10695. Wijesinghe, U.; Longo, G.; Hutter, O. S. Defect engineering in antimony selenide thin film solar cells. *Energy Adv.* **2023**, *2* (1), 12−33.

(4) Sahoo, N. K.; Apparao, K. V. S. R. Process-parameter optimization of Sb_2O_3 films in the ultraviolet and visible region for interferometric applications. *Appl. Phys. A: Mater. Sci. Process.* **1996**, *63* (2), 195−202.

(5) De Sande, J.; Vega, F.; Afonso, C. N.; Ortega, C.; Siejka, J. Optical properties of Sb and SbO_x films. *Thin Solid Films* **1994**, *249* (2), 195−200.

(6) Binions, R.; Carmalt, C. J.; Parkin, I. P. Antimony oxide thin films from the atmospheric pressure chemical vapour deposition reaction of antimony pentachloride and ethyl acetate. *Polyhedron* **2006**, *25* (15), 3032−3038.

(7) Arsat, R.; Tan, S. J.; Wlodarski, W.; Kalantar-Zadeh, K. Hydrogen gas sensor based on Sb_xO_y nanostructures with a langasite substrate. *Sens. Lett.* **2006**, *4* (4), 419−425.

(8) Yang, K.; Zhang, T.; Wei, B.; Bai, Y.; Jia, S.; Cao, G.; Jiang, R.; Zhang, C.; Gao, E.; Chang, X.; et al. Ultrathin high-κ antimony oxide single crystals. *Nat. Commun.* **2020**, *11* (1), 2502. Messalea, K. A.; Syed, N.; Zavabeti, A.; Mohiuddin, M.; Jannat, A.; Aukarasereenont, P.; Nguyen, C. K.; Low, M. X.; Walia, S.; Haas, B.; et al. High-k 2D Sb_2O_3 Made Using a Substrate-Independent and Low-Temperature Liquid-Metal-Based Process. *ACS Nano* **2021**, *15* (10), 16067−16075.

(9) Yang, J.; Bahrami, A.; Ding, X.; Zhao, P.; He, S.; Lehmann, S.; Laitinen, M.; Julin, J.; Kivekäs, M.; Sajavaara, T.; et al. Low-Temperature Atomic Layer Deposition of High-*k* SbO_x for Thin Film Transistors. *Adv. Electron. Mater.* **2022**, *8* (7), 2101334.

(10) Gheorghieş, C.; Gheorghieş, L. Characterization of the Sb_2O_3 thin films by X-ray scattering. *J. Optoelectron. Adv. Mater.* **2001**, *3* (2), 571−574.

(11) Tigau, N.; Ciupina, V.; Prodan, G.; Rusu, G.; Gheorghies, C.; Vasile, E. Structure and optical properties of thermally vacuum evaporated Sb_2O_3 thin films. *J. Optoelectron. Adv. Mater.* **2004**, *6*, 449−458.

(12) Mittov, O.; Ponomareva, N.; Mittova, I. Y. Metalorganic chemical vapor deposition of antimony oxide films on semiconductor substrates. *Inorg. Mater.* **2002**, *38*, 576−581.

(13) Yang, R. B.; Bachmann, J.; Reiche, M.; Gerlach, J. r. W.; Gösele, U.; Nielsch, K. Atomic layer deposition of antimony oxide and antimony sulfide. *Chem. Mater.* **2009**, *21* (13), 2586−2588.

(14) Kalkofen, B.; Mothukuru, V. M.; Klingsporn, M.; Burte, E. P. Investigation of antimony oxide films deposited by atomic layer deposition. *ECS Trans.* **2012**, *45* (3), 461.

(15) Ritala, M.; Leskelä, M. Chapter 2 - Atomic layer deposition. In *Handbook of Thin Films*; Singh Nalwa, H., Ed.; Academic Press, 2002; pp 103−159.

(16) Horley, G. A.; Mahon, M. F.; Molloy, K. C.; Venter, M. M.; Haycock, P. W.; Myers, C. P. Structures of $Sb(OC_6H_3Me_2\text{-}2,6)_3$ and $Sb(OEt)_5{\cdot}NH_3$: The First Authenticated Monomeric $Sb(OR)_n$ (n = 3, 5). *Inorg. Chem.* **2002**, *41* (6), 1652−1657.

(17) Horley, G. A.; Mahon, M. F.; Molloy, K. C.; Haycock, P. W.; Myers, C. P. Synthesis and characterization of novel homoleptic *N, N*-dialkylcarbamato complexes of antimony: Precursors for the deposition of antimony oxides. *Inorg. Chem.* **2002**, *41* (20), 5052−5058.

(18) George, S. M.; Nam, J. H.; Lee, G. Y.; Han, J. H.; Park, B. K.; Kim, C. G.; Jeon, D. J.; Chung, T.-M. *N*-Alkoxy Carboxamide Stabilized Tin(II) and Germanium(II) Complexes for Thin-Film Applications. *Eur. J. Inorg. Chem.* **2016**, *2016* (36), 5539−5546.

(19) Lee, G. Y.; Yeo, S.; Han, S. H.; Park, B. K.; Eom, T.; Kim, J. H.; Kim, S.-H.; Kim, H.; Son, S. U.; Chung, T.-M. Group IV Transition Metal (M = Zr, Hf) Precursors for High-κ Metal Oxide Thin Films. *Inorg. Chem.* **2021**, *60* (23), 17722−17732.

(20) Han, S. H.; Agbenyeke, R. E.; Lee, G. Y.; Park, B. K.; Kim, C. G.; Eom, T.; Son, S. U.; Han, J. H.; Ryu, J. Y.; Chung, T.-M. Novel Heteroleptic Tin(II) Complexes Capable of Forming SnO and SnO_2 Thin Films Depending on Conditions Using Chemical Solution Deposition. *ACS Omega* **2022**, *7* (1), 1232−1243. Lee, J. H.; Jung, E. A.; Lee, G. Y.; Han, S. H.; Park, B. K.; Lee, S. W.; Son, S. U.; Kim, C. G.; Chung, T.-M. Synthesis of Indium Complexes for Thin Film Transistor Applications Bearing *N*-Alkoxy Carboxamide Ligands. *ChemistrySelect* **2018**, *3* (23), 6691−6695. Yoo, D.; Han, S. H.; Lee, S. K.; Eom, T.; Park, B. K.; Kim, C. G.; Son, S. U.; Chung, T.-M. Synthesis of New Heteroleptic Indium Complexes as Potential Precursors for Indium Oxide Thin Films. *Eur. J. Inorg. Chem.* **2021**, *2021* (25), 2480−2485. Hwang, J. M.; Kim, N. Y; Shin, S.; Lee, J. H.; Ryu, J. Y; Eom, T.; Park, B. K; Kim, C. G; Chung, T.-M. Synthesis of novel volatile niobium precursors containing carboxamide for Nb_2O_5 thin films. *Polyhedron* **2021**, *200*, 115134. Hwang, J. M.; Lee, S. K.; Shin, S.; Jeong, J.-S.; Kim, H. S.; Ryu, J. Y.; Eom, T.; Park, B. K.; Kim, C. G.; Chung, T.-M. New Volatile Tantalum Imido Precursors with Carboxamide Ligands. *ACS Omega* **2021**, *6* (38), 24795−24802. Choi, H.; Park, C.; Lee, S. K.; Ryu, J. Y.; Son, S. U.; Eom, T.; Chung, T.-M. New Heteroleptic Germanium Precursors for GeO_2 Thin Films by Atomic Layer Deposition. *ACS Omega* **2023**, *8* (46), 43759−43770.

(21) Hoskins, B. F.; Tiekink, E. R. T.; Winter, G. The crystal and molecular structure of O-ethylxanthato-bis(quinolin-8-olato)-antimony(III) and a redetermination for tris(O-ethylxanthato)-antimony(III). *Inorg. Chim. Acta* **1985**, *97* (2), 217−222.

(22) Horley, G. A.; Mahon, M. F.; Mazhar, M.; Molloy, K. C.; Haycock, P. W.; Myers, C. P. Antimony *β*-diketonates and alkoxide/*β*-diketonates: remarkable formation of a 3,4-dihydro-2*H*-pyran ring by coupling of 1,1,1,5,5,5-hexafluoro-2,4-pentanedione ligands. *J. Chem. Soc., Dalton Trans.* **2002**, No. 23, 4416−4421.

(23) Lee, C.; Yang, W.; Parr, R. G. Development of the Colle-Salvetti correlation-energy formula into a functional of the electron density. *Phys. Rev. B* **1988**, *37* (2), 785−789.

(24) Hariharan, P. C.; Pople, J. A. The influence of polarization functions on molecular orbital hydrogenation energies. *Theor. Chim. Acta* **1973**, *28* (3), 213−222.

(25) Stevens, W. J.; Krauss, M.; Basch, H.; Jasien, P. G. Relativistic compact effective potentials and efficient, shared-exponent basis sets for the third-, fourth-, and fifth-row atoms. *Can. J. Chem.* **1992**, *70* (2), 612−630.

(26) Young, J. A. Antimony(III) Chloride. *J. Chem. Educ.* **2003**, *80* (6), 611.

(27) https://www.upchem.co.kr/product/use1_semic1_6.php?ptype=view&prdcode=1112160040&catcode=101015&page=1&catcode=101015&searchopt=&searchkey=.

(28) Eom, T.; Gwon, T.; Yoo, S.; Choi, B. J.; Kim, M.-S.; Ivanov, S.; Adamczyk, A.; Buchanan, I.; Xiao, M.; Hwang, C. S. Chemical interaction and ligand exchange between a $[(CH_3)_3Si]_3Sb$ precursor and atomic layer deposited Sb_2Te_3 films. *J. Mater. Chem. C* **2015**, *3* (6), 1365−1370.

(29) Morávek, P.; Fulem, M.; Pangrác, J.; Hulicius, E.; Růžička, K. Vapor pressures of dimethylcadmium, trimethylbismuth, and tris-(dimethylamino)antimony. *Fluid Phase Equilib.* **2013**, *360*, 106−110.

(30) Banjo, S.; Nakasuji, E.; Meguro, T.; Sato, T.; Chida, N. Copper-Catalyzed Electrophilic Amidation of Organotrifluoroborates with Use of *N*-Methoxyamides. *Chem.—Eur. J.* **2019**, *25* (33), 7941−7947.

(31) Bruker, A. *APEX2*, version 2011; Bruker AXS Inc., Madison, Wisconsin, USA, 2011.

(32) Krause, L.; Herbst-Irmer, R.; Sheldrick, G. M.; Stalke, D. Comparison of silver and molybdenum microfocus X-ray sources for single-crystal structure determination. *J. Appl. Crystallogr.* **2015**, *48* (1), 3−10.

(33) Sheldrick, G. M. Crystal structure refinement with SHELXL. *Acta Crystallogr., Sect. C: Struct. Chem.* **2015**, *71* (1), 3−8.

(34) Dolomanov, O. V.; Bourhis, L. J.; Gildea, R. J.; Howard, J. A. K.; Puschmann, H. OLEX2: a complete structure solution, refinement and analysis program. *J. Appl. Crystallogr.* **2009**, *42* (2), 339−341.

(35) *Gaussian 16*, Rev. C.01; Wallingford, CT, 2016.

https://doi.org/10.1021/acsomega.4c03482
ACS Omega 2024, 9, 31871−31877